Oxidative addition or Werner coordination complex? Reactivity of β-diketiminate supported main group and first-row transition metal complexes towards ammonia†

Petra Vasko [ID] * and Cheuk W. Lau

A series of neutral **LM** (L = [HC{(H₃C)C(Dipp)N}₂], Dipp = 2,6-ⁱPr₂C₆H₃, M = group 13: B–In, TM: Fe, Co, Ni, Cu) and **L'M** (L' = [HC{(C=CH₂)(CCH₃)(DippN)₂}], M = group 14: C–Pb) compounds including a main group 13/14 and first-row transition metal complexes were studied computationally by density functional theory (DFT). The optimised complexes were assessed in terms of structural parameters and electronic structures to find trends and characteristics that could be used to predict their reactivity towards ammonia. In addition, the differences in oxidative addition and Werner coordination complex formation depending on the identity of the central element were investigated and the Werner complexes were evaluated by QTAIM and EDA-NOCV approaches. The computational results complement the earlier experimental studies and shed light on the feasibility of isolating novel main group Werner complexes or transition metal oxidative addition products.

Introduction

In the last few decades, the main group chemistry community has proven that p-block element containing species can achieve reactivity that was previously thought to be the sole domain of transition metal complexes.[1,2] A recent example of this is the first main group compound to activate dinitrogen, published by Braunschweig and co-workers.[3] Furthermore, in the realm of small molecule activation, main group compounds have shown excellent, and in some cases reversible, reactivity towards inert molecules such as H₂,[4,5] CO₂[6] and NH₃.[7] The preferred mode of reactivity for low-valent p-block species is oxidative addition. However, as this usually results in highly stable thermodynamic products, achieving reversibility through reductive elimination is in most cases impossible. One of the big challenges for main group chemists is, in fact, evaluating the structure and reactivity relationships between the complexes/catalysts and substrates to achieve efficient and applicable catalysis with high turnover numbers and frequencies.[8]

In contrast to main group species, transition metal complexes are known for their performance in catalytic applications: the wide range of accessible oxidation states and energetically close frontier molecular orbitals ensure the reversibility of the oxidative addition–reductive elimination catalytic cycle. However, there are reactions that even transition metal complexes struggle with: the activation of ammonia to produce an oxidative addition product instead of a classical Werner coordination complex is a challenge. Thus far, only one complex has been observed to react with ammonia to produce an amido hydride product: Hartwig *et al.* isolated a RIr(H)NH₂-complex (R = 1,5-bis(di-*t*-butylphosphino)pentan-3-yl) following a reaction of RIr(CH₂CHCH₃) with ammonia under ambient conditions.[9]

Due to these interesting differences in reactivity with ammonia, we set out to perform a series of computational analyses to investigate the characteristics of main group 13/14 compounds and first-row transition metal complexes stabilised by the ubiquitous β-diketiminate ligand (L, group 13 and TM) or its deprotonated derivative (L', group 14) (Fig. 1). In addition, we attempted to clarify the nature of the metal–ammonia nitrogen bond in the calculated Werner coordination complexes by QTAIM and EDA-NOCV analyses.

Department of Chemistry, University of Helsinki, A. I. Virtasen aukio 1, P.O. Box 55, 00014 Helsinki, Finland. E-mail: petra.vasko@helsinki.fi

†Electronic supplementary information (ESI) available: Additional computational details and optimized *xyz*-coordinates of the structures. See DOI: https://doi.org/10.1039/d2dt02427f
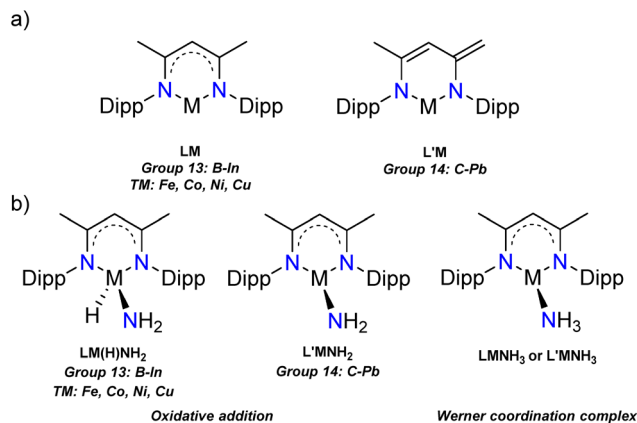
Computational details

All DFT optimizations were performed using Gaussian16 Rev. C.01 programme[10] with PBE1PBE hybrid exchange–correlation functional[11–13] in combination with Def2-TZVP[14,15] basis set.

a)

b)

Fig. 1 (a) The neutral complexes **LM** and **L′M** studied in this work, (b) two activation modes of the **LM/L′M** species towards ammonia (Dipp = 2,6-^{i}Pr$_2$C$_6$H$_3$).

Table 1 A summary of the key calculated **LM/L′M** bond parameters

Compound	M–N (Å)		N–M–N (°)	M–N–C–C (°)
LFe	1.869	1.794	94.8	5.1
LCo	1.949	1.891	99.8	−13.3
LNi	1.871	1.870	105.3	−0.5
LCu	1.880	1.881	114.2	−0.3
LB	1.449	1.449	113.6	24.5
LAl	1.993	1.988	88.5	−5.3
LGa	2.079	2.079	86.6	0.0
LIn	2.308	2.307	80.7	−2.3
L′C	1.352	1.341	114.8	1.3
L′Si	1.750	1.736	98.6	0.0
L′Ge	1.869	1.852	95.8	−0.0
L′Sn	2.068	2.047	90.6	0.0
L′Pb	2.168	2.143	88.2	−0.0

In addition, Grimme's empirical dispersion correction with Becke–Johnson damping (GD3BJ)[16] and an ultrafine integration grid were applied. For In, Sn and Pb a pseudopotential (ECP) was used to model the core electrons. Full frequency calculations were performed to the optimised structures to ensure the identity of the stationary points on the potential energy surface (no imaginary frequencies). The Gaussian optimised structures were further used for QTAIM and EDA-NOCV analyses. QTAIM analyses were done using the programme AIMAll[17] and EDA-NOCV[18–20] calculations using ADF programme[21] (PBE0/TZ2P, numerical quality good, no symmetry and no frozen core except ZORA[22–24] for In, Sn and Pb). All optimisations were performed in the gas phase and the calculated energies are given in kJ mol^{-1}.

Results and discussion

Geometry optimisations and electronic structures

We began our investigations by optimising the **LM** (L = Nacnac or β-diketiminate, [HC{(H$_3$C)C(Dipp)N}$_2$], Dipp = 2,6-^{i}Pr$_2$C$_6$H$_3$, M = group 13: B–In, and TM: Fe, Co, Ni, Cu) and **L′M** (L′ = [HC{(C═CH$_2$)(CCH$_3$)(DippN)$_2$}], M = group 14: C–Pb) (Fig. 1a) species and their ammonia reaction products, amido hydrides and Werner adducts (Fig. 1b), by density functional theory (DFT). We chose the Nacnac-framework as our supporting ligand because of its extensive experimental use and modest size to facilitate efficient computational resource usage. Moreover, a variety of Nacnac-ligands and their deprotonated derivatives have been shown to stabilise a wide range of both main group and first-row transition metal compounds in the past.[25–27] In our study, the main group elements were treated to bear either +I (group 13) or +II (group 14) formal charge to ensure the overall neutral compounds. For the first-row transition metals, we decided to examine **LM** complexes where the formal charge of the metal is +I (M = Fe, Co, Ni, and Cu). This results in neutral paramagnetic Fe (multiplicity doublet), Co

(multiplicity triplet) and Ni (multiplicity doublet) complexes, which may not be isolable experimentally but in our study provide interesting comparison to the main group species.[25] The optimised **LM** and **L′M** geometries show, that, firstly, the calculated gas phase structures are in good agreement with the structurally characterised ones found in the Cambridge structural database (M = Al,[28] Ga,[29] In,[30] Si,[31,32] and Ge[7,33] see ESI† for structural comparison). Secondly, the optimised geometries show expected trends in the bond parameters corresponding to the size of the element M: the N–M bond lengths increase going down the groups 13 and 14, and, as expected, there is slightly more variation in the N–M bonds for the group 14 and transition metal species (Table 1). The N–M–N angle decreases going down the groups 13 and 14, most likely due to the increasing lone pair s-character of the heavier analogues. The more acute bond angles also explain the long N–M bonds observed for the heavy group 13 and 14 compounds. However, the transition metal compound structures show less clear trends in the bonding; the M–N bond lengths are significantly shorter than the sum of covalent radii[37] of the two elements and the N–M–N angle varies from 94.8° in Fe to 114.2° in the Cu complex. The observed transition metal structural features might be due to the assumed two-coordinate bonding mode in the **LM/L′M** complexes.

Majority of the optimised structures show either planar or near planar arrangements of the Nacnac-heterocycle, one main group exception being **LB**, which exhibits a highly twisted structure and a B–N–C–C dihedral angle of 24.5°. The boron structure can be explained by a very narrow HOMO–LUMO gap (*vide infra*). Another interesting geometry can be observed for the transition metal analogue **LCo**, which exhibits a close contact between the Co–metal and Dipp-substituent's methyl hydrogen (1.871 Å). This close contact twists the heterocycle from planarity which results in a Co–N–C–C dihedral angle of −13.3°.

Next, we turned our attention to evaluating the electronic structures of the **LM/L′M** complexes. In especially main group chemistry, the magnitude of the HOMO–LUMO gap (or singlet–triplet gap) can be used to evaluate the relative stability and/or reactivity of the compound. Especially for low valent
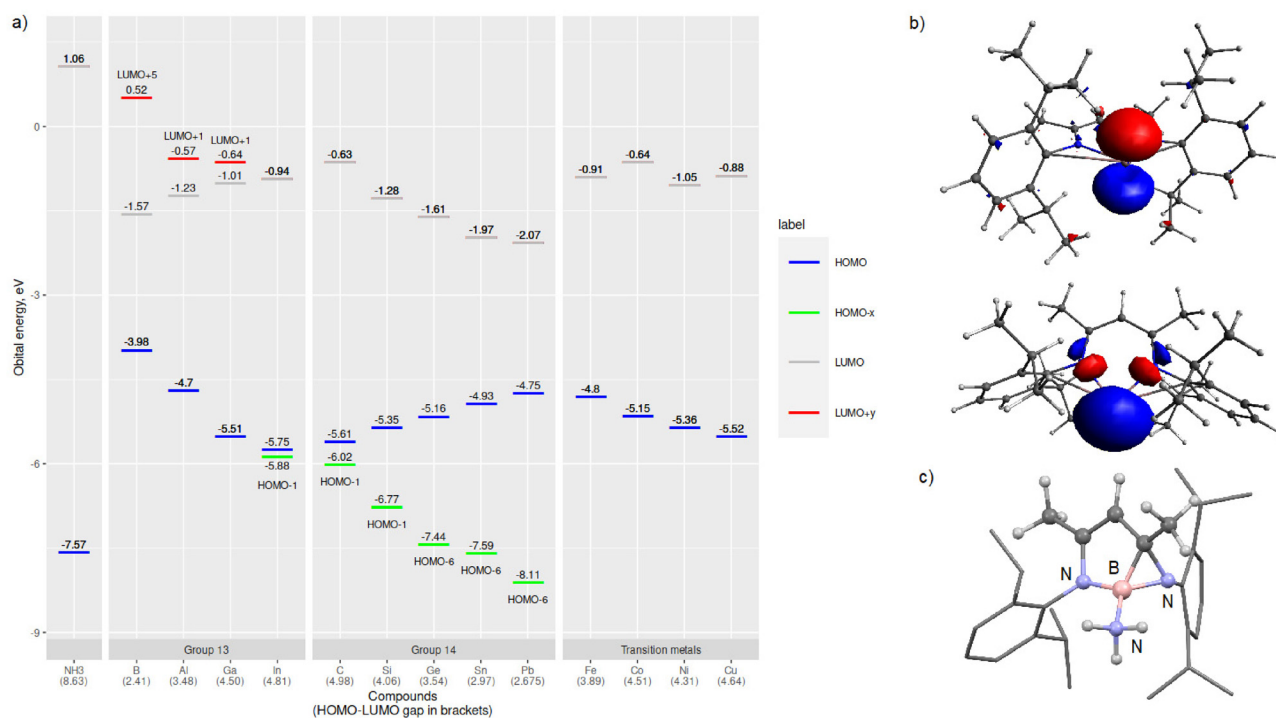
Fig. 2 (a) Calculated HOMO−x and LUMO+y energy levels for the computed **LM/L′M** species. HOMO−x indicates a lone pair MO and LUMO+y an empty p-orbital associated with the main group element M, (b) LUMO+1 (upper) and HOMO (lower) of **LGa** (isovalue set at ±0.05 a.u.), and (c) structure of the rearranged **LB·NH₃**, Dipp-groups are shown as a wireframe format for clarity.

group 13 and 14 species, the HOMO is usually the lone electron pair and LUMO the empty p-orbital, exactly the frontier molecular orbitals involved in formal oxidative addition or adduct forming reactions. Fig. 2 includes a graph of the calculated frontier molecular orbital (FMO) energies of the **LM/L′M** complexes and an illustration of the **LGa** HOMO and LUMO+1 orbitals. The calculated HOMO–LUMO gaps for the **LM/L′M** complexes vary from 2.41 (**LB**) to 4.98 eV (**L′C**). For the group 13 compounds, the HOMO–LUMO gap widens in going down the group due to more stabilised HOMO (lower in energy) and at the same time destabilised LUMO (higher in energy). The opposite holds for group 14; the HOMO–LUMO gap gets narrower when the group is descended. However, a closer look at the FMOs reveals that in fact for group 14, the HOMO is a ligand-backbone related bonding orbital and not the group 14 element based lone pair orbital. That said, when the orbital energy gap between the central element lone pair (HOMO−x) and the empty p-orbital (LUMO) is computed, the trends are similar in both groups 13 and 14. For the first row transition metal complexes, the HOMO/SOMO includes a contribution from one of the metal associated 3d-orbitals and Nacnac-backbone while the LUMO is mainly an empty d-orbital (4s-orbital for M = Ni and Cu). In general, the HOMO(−x)–LUMO(+y) gaps are wider for the main group species than for the transition metal complexes.

Reactivity towards ammonia

Based on the electronic structure alone, a mode of reactivity between the **LM/L′M** compounds and ammonia can be evalu-

ated. The Werner coordination complex formation involves the interaction between the **LM/L′M** empty p-orbital (groups 13 and 14) or 3d/4s-orbital (transition metals) and the lone pair of nitrogen in ammonia. To achieve oxidative addition, one of the N–H bonds in ammonia needs to be cleaved, which involves the additional participation of the central element M lone pair (Fig. 3). There are few excellent computational studies on the mechanism of the oxidative addition of small molecules by main group species, and in the case of ammonia reacting with group 14 metallylenes, it is speculated that a proton shuttling mechanism involving two different ammonia molecules is the most probable one.[34–36] The involvement of two NH₃ molecules can lower the associated transition state significantly compared to a mechanism with only one ammonia moiety as there is no need for ammonia dissociation and the H transfer is stabilised by the involvement of the second ammonia molecule. Because of these already published studies on the mechanism of ammonia activation by
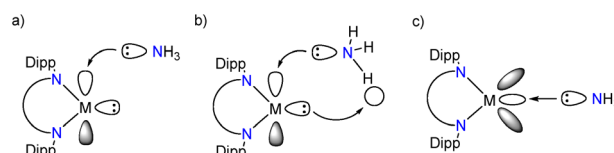

Fig. 3 Frontier molecular orbital interactions of **LM** and NH₃ to form (a) Werner adduct (M = main group element), (b) amido hydride (M = main group element) and (c) Werner adduct (M = transition metal).

main group species, we focussed our efforts on investigating the reasons that result in the different modes of reactivity (*vide infra*).

In the main group **LM/L′M** compounds a highly stabilised HOMO and a wide HOMO–LUMO gap would indicate a relatively unreactive main group element based lone pair. In consequence, this allows facile access to the empty p-orbital (LUMO, provided the ammonia FMO orbital energies match) and hence pronounced tendency to form the ammine adduct **LM·NH₃**. As the lone pair orbital (HOMO−*x*) and empty p-orbital (LUMO+*y*) get closer in energy, the compound will become more reactive, and the oxidative addition product should become more favourable. To assess this hypothesis, the oxidative addition products, **LM(H)NH₂** (M = group 13 or Fe, Co, Ni, Cu) or **LMNH₂** (M = group 14) and ammine adducts, **LM·NH₃/L′M·NH₃**, were optimised computationally. To our knowledge there are only two isolated examples of a reaction between **L′M** moiety and ammonia reported in the literature: silicon and germanium oxidative addition products **L′Si(H) NH₂** [32] and **LGeNH₂**.[7] The comparison of experimental and calculated bond parameters revealed an excellent agreement of the data (see ESI†).

Furthermore, a closer look at the optimised structures of the **LM** amido hydrides and ammine adducts revealed expected trends and few anomalies. Unsurprisingly, the **L′C** species does not bind ammonia as the C–N interaction is measured to be over 4.29 Å in the optimised adduct structure. In addition, **LB** rearranges to a five-membered ring upon reaction with ammonia (Fig. 2c). Both of these observations can be explained by the narrowest (M = B) and widest (M = C) HOMO–LUMO gaps computed for the whole series (Fig. 2). In addition, the boron-compound rearrangement is probably further facilitated by the non-planar structure of **LB** (*vide supra*). The calculated main group **LM/L′M** and ammonia nitrogen M–N interactions in the ammine adducts are significantly longer than the sum of the covalent radii of the two elements (Table 3).[37] In contrast, the M–N$_{NH_3}$ bonding interaction is clearly shorter in the computed transition metal ammine adducts as expected based on the electrophilicity of the 3d-metals.

All optimised structures at hand, we began our analyses by comparing the Gibbs free energies of the reactions resulting in either the oxidative addition product or the Werner adduct (Table 2). For the group 14 compounds, we examined the relative energies of both the 1,1- and 1,4-addition products **L′M(H)NH₂** and **LMNH₂** where the proton has migrated to the Nacnac-backbone methine carbon. In line with the experimental observations and the calculated frontier molecular orbital energies,[7,32,36] the 1,1-addition was preferred for the carbene and silylene analogues whereas for the other elements M = Ge, Sn and Pb, the 1,4-addition product was more stable. The oxidative addition products were found to be the thermodynamic product for group 13 and 14 compounds, except for **LIn**, for which both reactions were calculated to be endergonic. The unfavourable oxidative addition reaction for **LIn** can be explained by the inaccessibility and high energy level of the

Table 2 A summary of the Gibbs free energy change in kJ mol⁻¹ for oxidative addition *vs.* Werner adduct formation between **LM/L′M** and NH₃

Compound	Oxidative addition	Werner adduct
LFe	−66.5	−97.2
LCo	7.8	−82.8
LNi	64.8	−73.6
LCu	129.0	−66.7
LB	−260.4	−82.1
LAl	−173.6	23.8
LGa	−34.6	31.3
LIn	73.6	15.7
L′C	−67.3[a]	9.8
L′Si	−126.6[a]	25.6
L′Ge	−46.8[b]	15.8
L′Sn	−70.1[b]	−8.6
L′Pb	−66.2[b]	−9.9

[a] The 1,1-addition product without proton transfer to the ligand backbone methine carbon is the lowest energy structure. [b] The 1,4-addition product.

LUMO. The transition metal congeners expectedly exhibit the opposite reactivity: the Werner coordination complex is the thermodynamic product for all M = Fe, Co, Ni and Cu Nacnac-complexes. Interestingly, the 1,1-addition reaction for **LFe** was calculated to be exergonic by −66.5 kJ mol⁻¹, indicating that with the correct ligand system and reaction conditions, an amido hydride product might be isolable for Fe-complex.

According to the data in Table 2, it is likely that all of the studied transition metal complexes can form a stable Werner adduct with ammonia. Moreover, the calculations indicate that the oxidative addition products could be isolable for all main group **LM/L′M** species (except for M = In). Interestingly, the data also suggests that the Werner coordination compounds might be isolable for the main group species M = B, Sn and Pb, for which the adduct is the kinetic product of the reaction between the complex and ammonia. This, however, would require a careful optimisation of reaction conditions and maybe further tuning of the ligand sterics and electronics.

The calculated Werner coordination complex structures, along with the Gibbs free energy calculations of the reactions, suggest that the ammonia moiety in the Werner adducts is more tightly bound in the transition metal complexes than in main group species. To further probe this and the nature of the ammonia adducts and the M–N interactions, we utilised the QTAIM method: the Bader charges of the element M (q(A)) and ammonia nitrogen (q(B)) were calculated as well as the bonding critical point (BCP) properties between the two atoms to shed light on the favourability of the ammine adduct formation depending on the metal M. These results are summarised in Table 3. The calculated atomic charges reveal that the ammonia nitrogen carries a significant negative charge in all adducts as expected based on electronegativities of the atoms.[38] The element M, however, is oxidised to a varying extent: group 14 elements carry calculated charges greater than +1 (with C as an exception) and group 13 less than +1

Table 3 A summary of the QTAIM analyses of the ammine adducts of **LM/L′M**. Bond critical point (BCP) properties are given for the complex M–N_{NH_3} bond

Compound	$q(A)$	$q(B)$	$\rho(r_{bcp})$ (e Å^{-3})	$\nabla^2\rho(r_{bcp})$ (e Å^{-5})	DI (A|B)	d(A–B)^b (Å)
LFe·NH₃	+0.76	−1.13	0.0766	0.3210	0.5324	2.064 (2.03)
LCo·NH₃	+0.69	−1.12	0.0801	0.3342	0.5336	2.046 (1.97)
LNi·NH₃	+0.63	−1.10	0.0818	0.3813	0.5562	2.014 (1.95)
LCu·NH₃	+0.61	−1.09	0.0856	0.3674	0.5536	2.005 (2.03)
LB·NH₃	+2.05	−1.25	0.1341	0.3505	0.3449	1.581 (1.55)
LAl·NH₃	+0.98	−1.22	0.0394	0.1187	0.2794	2.223 (1.92)
LGa·NH₃	+0.67	−1.12	0.0308	0.0541	0.2577	2.555 (1.93)
LIn·NH₃	+0.68	−0.11	0.0296	0.0758	0.2620	2.678 (2.13)
L′C·NH₃^a	+0.90	−1.08	—	—	0.0007	4.294 (1.47)
L′Si·NH₃	+1.61	−1.22	0.0635	0.0800	0.3595	2.101 (1.82)
L′Ge·NH₃	+1.19	−1.14	0.0607	0.0910	0.4052	2.243 (1.91)
L′Sn·NH₃	+1.20	−1.15	0.0494	0.1170	0.3764	2.436 (2.10)
L′Pb·NH₃	+1.14	−1.13	0.0451	0.1134	0.3614	2.549 (2.17)

^{a} No BCP was found between C and N. ^{b} Sum of covalent radii according to ref. 37.

(with B as an exception). The transition metals all carry a positive charge less than +1. A bond critical point for the bond M–N_{NH_3} was located for all **LM/L′M** complexes, except for M = C. The calculated BCP properties reveal that the electron density at the BCP is very small and has very little covalent character (Laplacian of ρ is small and positive, positive values indicate depletion of electron density at the BCP and are generally related to electrostatic or non-covalent type interactions) in the main group species.[39] However, the values grow for M = Fe, Co, Ni and Cu, indicating stronger bonding between the two moieties. This is further corroborated by the greater delocalisation indices, DI(A|B) for the transition metal complexes as DI(A|B) can be used to evaluate the bond order.[40]

The final bonding analysis we performed for the Werner adducts was the energy decomposition analysis (EDA) in combination with the natural orbitals for chemical valence formalism (NOCV). The EDA-NOCV analysis used the neutral **LM/L′M** and NH₃ fragments as optimised in the respective ammine adducts. The total instantaneous interaction energies were found to range from −43.2 (Ga) to −174.2 kJ mol^{-1} (Ni) (Table 4). Consistent with the QTAIM results, the **LM/L′M** and

ammine interactions are strongest for the transition metal analogues. A breakdown of the total interaction energies to repulsive (Pauli repulsion) and attractive (electrostatic, orbital and dispersion interactions) components reveals, that for the transition metal complexes the Pauli repulsion is offset completely by the electrostatic interactions and thus the orbital interactions are the biggest contributor to the total interaction energy. The dispersion component is of similar magnitude for the whole series but becomes more important in stabilising the adducts for the main group species because the Pauli repulsion term is significantly greater than the electrostatic interaction for the group 13 and 14 species. Furthermore, the relatively small orbital interaction values for the M–N_{NH_3} bonds support the non-covalent description from the QTAIM analysis (*vide supra*).

Finally, a closer look at the orbital interactions reveals that the major component in the M–N bonding is composed of the charge flux from the ammonia nitrogen to the element M as expected. For example for the main group adducts, this charge flow constitutes roughly 70% of the overall orbital interactions calculated for the species (see ESI† for further details).

Table 4 A summary of the key results of energy decomposition analysis (EDA) of the ammine adducts of **LM/L′M** given in kJ mol^{-1}.^{a}

	Pauli repulsion	Electrostatic interaction	Orbital interactions	Dispersion	Total
LFe·NH₃	296.5	−296.5	−132.5	−19.4	−152.0
LCo·NH₃	315.9	−308.4	−122.5	−15.5	−130.5
LNi·NH₃	298.4	−302.7	−151.0	−18.9	−174.2
LCu·NH₃	299.0	−305.6	−109.9	−18.5	−134.9
LAl·NH₃	349.0	−245.8	−136.3	−17.2	−50.3
LGa·NH₃	157.9	−114.9	−67.3	−18.9	−43.2
LIn·NH₃	143.7	−115.9	−60.3	−16.9	−49.1
L′Si·NH₃	499.4	−325.0	−235.3	−21.5	−82.4
L′Ge·NH₃	381.9	−265.0	−175.6	−20.3	−79.0
L′Sn·NH₃	293.0	−229.4	−134.2	−19.3	−89.8
L′Pb·NH₃	235.2	−195.2	−108.6	−20.3	−89.0

^{a} **LB** and **L′C** were excluded from this analysis due to their different reactivity with ammonia to the rest of the series.

Conclusions

A computational approach to study the reactivity of main group 13/14 and first-row transition metal **LM**/**L′M** complexes towards ammonia was exploited. First, the optimised structures were evaluated in terms of their electronic structures and frontier molecular orbital energies to reveal trends in compound stability and reactivity. Next, the difference in reactivity towards ammonia was investigated and as expected, the transition metal complexes were found to prefer the formation of a classical Werner coordination complex over an oxidative addition product. For main group species the reactivity was observed to be the opposite. However, the formation energies along with QTAIM and EDA-NOCV calculations suggest that the isolation of a Werner coordination complex of ammonia might be plausible for few main group element species (B, Sn and Pb), provided that the experimental conditions are optimised.

Author contributions

PV: conceptualization, methodology, data curation, funding acquisition, supervision, resources, project administration, writing – original draft, review and editing; CWL: data curation and analysis.

Conflicts of interest

There are no conflicts to declare.

Acknowledgements

References

1 P. P. Power, *Nature*, 2010, **463**, 171–177.
2 C. Weetman and S. Inoue, *ChemCatChem*, 2018, **10**, 4213–4228.
3 M.-A. Légaré, G. Bélanger-Chabot, R. D. Dewhurst, E. Welz, I. Krummenacher, B. Engels and H. Braunschweig, *Science*, 2018, **359**, 896–900.
4 J. Hicks, P. Vasko, J. M. Goicoechea and S. Aldridge, *Nature*, 2018, **557**, 92–95.
5 G. C. Welch, R. R. S. Juan, J. D. Masuda and D. W. Stephan, *Science*, 2006, **314**, 1124–1126.
6 A. V. Protchenko, P. Vasko, D. C. H. Do, J. Hicks, M. Á. Fuentes, C. Jones and S. Aldridge, *Angew. Chem., Int. Ed.*, 2019, **58**, 1808–1812.
7 A. Jana, I. Objartel, H. W. Roesky and D. Stalke, *Inorg. Chem.*, 2009, **48**, 798–800.
8 O. Planas, F. Wang, M. Leutzsch and J. Cornella, *Science*, 2020, **367**, 313–317.
9 J. Zhao, A. S. Goldman and J. F. Hartwig, *Science*, 2005, **307**, 1080–1082.
10 M. J. Frisch, G. W. Trucks, H. B. Schlegel, G. E. Scuseria, M. A. Robb, J. R. Cheeseman, G. Scalmani, V. Barone, G. A. Petersson, H. Nakatsuji, X. Li, M. Caricato, A. V. Marenich, J. Bloino, B. G. Janesko, R. Gomperts, B. Mennucci, H. P. Hratchian, J. V. Ortiz, A. F. Izmaylov, J. L. Sonnenberg, D. Williams-Young, F. Ding, F. Lipparini, F. Egidi, J. Goings, B. Peng, A. Petrone, T. Henderson, D. Ranasinghe, V. G. Zakrzewski, J. Gao, N. Rega, G. Zheng, W. Liang, M. Hada, M. Ehara, K. Toyota, R. Fukuda, J. Hasegawa, M. Ishida, T. Nakajima, Y. Honda, O. Kitao, H. Nakai, T. Vreven, K. Throssell, J. A. Montgomery Jr., J. E. Peralta, F. Ogliaro, M. J. Bearpark, J. J. Heyd, E. N. Brothers, K. N. Kudin, V. N. Staroverov, T. A. Keith, R. Kobayashi, J. Normand, K. Raghavachari, A. P. Rendell, J. C. Burant, S. S. Iyengar, J. Tomasi, M. Cossi, J. M. Millam, M. Klene, C. Adamo, R. Cammi, J. W. Ochterski, R. L. Martin, K. Morokuma, O. Farkas, J. B. Foresman and D. J. Fox, *Gaussian 16 Rev. C.01*, Wallingford, CT, 2016.
11 J. P. Perdew, K. Burke and M. Ernzerhof, *Phys. Rev. Lett.*, 1996, **77**, 3865–3868.
12 J. P. Perdew, K. Burke and M. Ernzerhof, *Phys. Rev. Lett.*, 1997, **78**, 1396–1396.
13 C. Adamo and V. Barone, *J. Chem. Phys.*, 1999, **110**, 6158–6170.
14 F. Weigend and R. Ahlrichs, *Phys. Chem. Chem. Phys.*, 2005, **7**, 3297–3305.
15 F. Weigend, *Phys. Chem. Chem. Phys.*, 2006, **8**, 1057–1065.
16 S. Grimme, S. Ehrlich and L. Goerigk, *J. Comput. Chem.*, 2011, **32**, 1456–1465.
17 T. A. Keith, *AIMAll, TK Gristmill Software*, Overland Parks KS, USA, 2019.
18 T. Ziegler and A. Rauk, *Inorg. Chem.*, 1979, **18**, 1558–1565.
19 T. Ziegler and A. Rauk, *Inorg. Chem.*, 1979, **18**, 1755–1759.
20 M. P. Mitoraj, A. Michalak and T. Ziegler, *J. Chem. Theory Comput.*, 2009, **5**, 962–975.
21 G. te Velde, F. M. Bickelhaupt, E. J. Baerends, C. Fonseca Guerra, S. J. A. van Gisbergen, J. G. Snijders and T. Ziegler, *J. Comput. Chem.*, 2001, **22**, 931–967.
22 E. van Lenthe, E. J. Baerends and J. G. Snijders, *J. Chem. Phys.*, 1993, **99**, 4597–4610.
23 E. van Lenthe, E. J. Baerends and J. G. Snijders, *J. Chem. Phys.*, 1994, **101**, 9783–9792.
24 E. van Lenthe, A. Ehlers and E.-J. Baerends, *J. Chem. Phys.*, 1999, **110**, 8943–8953.
25 P. L. Holland, T. R. Cundari, L. L. Perez, N. A. Eckert and R. J. Lachicotte, *J. Am. Chem. Soc.*, 2002, **124**, 14416–14424.

26 T. R. Dugan, X. Sun, E. V. Rybak-Akimova, O. Olatunji-Ojo, T. R. Cundari and P. L. Holland, *J. Am. Chem. Soc.*, 2011, **133**, 12418–12421.

27 T. Chu, I. Korobkov and G. I. Nikonov, *J. Am. Chem. Soc.*, 2014, **136**, 9195–9202.

28 C. Cui, H. W. Roesky, H.-G. Schmidt, M. Noltemeyer, H. Hao and F. Cimpoesu, *Angew. Chem., Int. Ed.*, 2000, **39**, 4274–4276.

29 N. J. Hardman, B. E. Eichler and P. P. Power, *Chem. Commun.*, 2000, 1991–1992.

30 M. S. Hill and P. B. Hitchcock, *Chem. Commun.*, 2004, 1818–1819.

31 M. Driess, S. Yao, M. Brym, C. van Wüllen and D. Lentz, *J. Am. Chem. Soc.*, 2006, **128**, 9628–9629.

32 A. Jana, C. Schulzke and H. W. Roesky, *J. Am. Chem. Soc.*, 2009, **131**, 4600–4601.

33 M. Driess, S. Yao, M. Brym and C. van Wüllen, *Angew. Chem., Int. Ed.*, 2006, **45**, 4349–4352.

34 D. C. H. Do, A. V. Protchenko, M. Á. Fuentes, J. Hicks, P. Vasko and S. Aldridge, *Chem. Commun.*, 2020, **56**, 4684–4687.

35 Y. Peng, J.-D. Guo, B. D. Ellis, Z. Zhu, J. C. Fettinger, S. Nagase and P. P. Power, *J. Am. Chem. Soc.*, 2009, **131**, 16272–16282.

36 M. E. Alberto, N. Russo and E. Sicilia, *Chem. – Eur. J.*, 2013, **19**, 7835–7846.

37 B. Cordero, V. Gómez, A. E. Platero-Prats, M. Revés, J. Echeverría, E. Cremades, F. Barragán and S. Alvarez, *Dalton Trans.*, 2008, 2832–2838.

38 L. Pauling, *J. Am. Chem. Soc.*, 1932, **54**, 3570–3582.

39 G. Frenking and S. Shaik, *The Chemical Bond: Fundamental Aspects of Chemical Bonding*, John Wiley & Sons, Incorporated, Weinheim, GERMANY, 2014.

40 C. Outeiral, M. A. Vincent, Á. M. Pendás and P. L. A. Popelier, *Chem. Sci.*, 2018, **9**, 5517–5529.